Int J Adv Manuf Technol (2013) 66:1427–1437
DOI 10.1007/s00170-012-4420-9

ORIGINAL ARTICLE

Microstructure evolution modeling of titanium alloy large ring in hot ring rolling

Min Wang · He Yang · Chun Zhang · Liang-gang Guo

Received: 18 December 2011 / Accepted: 24 July 2012 / Published online: 16 August 2012

Abstract Exploration of microstructure evolution is of significance for manufacturing the large ring with high performance and high reliability in hot ring rolling. In the study, the microstructure evolution model and the rate-/temperature-/microstructure-dependent constitutive model of titanium alloy are implemented in ABAQUS/Explicit through the user material subroutine VUMAT. The developed subroutine is validated by single-element models and isothermal upsetting experiments of Ti–6Al–4V cylinder. The subroutine is imbedded into a coupled thermomechanical three-dimensional finite element (3D-FE) model for hot rolling of Ti–6Al–4V large ring. The evolution characteristics of β phase volume fraction and grain size of Ti–6Al–4V during the process are revealed, and the final microstructures of the large ring under different processing conditions are explored. The results obtained show that (1) microstructure evolution follows the trend with the process progressing: the fine grain zone transfers from the surface layer (SL) to the middle layer (ML) of the ring; the poor β zone extends from the outside of the SL to the end-plane of the ML, and the rich β zone always locates at the SL. (2) decreasing the rotational velocity of the driver roll n_1, or increasing the feed rate of the idle roll v or the initial temperature of the ring T_0 contributes to more uniform distributions of β phase and its grain size, but results in the increase of the β phase volume fraction and grain size.

M. Wang (✉) · C. Zhang
Department of Material Engineering,
Hubei University of Automotive Technology,
Shiyan 442002, China
e-mail: sprit418@mail.nwpu.edu.cn

M. Wang · H. Yang · L.-g. Guo
School of Material Science and Engineering,
Northwestern Polytechnical University,
Xi'an 710072, China

Keywords Titanium alloy · Large ring · Hot ring rolling · Microstructure evolution · FEM

1 Introduction

Large seamless rings, key components of airplane, spacecraft, and rocket, are widely used in high-tech fields such as aviation and space industries. This type of rings is now produced mainly by hot ring rolling, an advanced rotary forming technology characterized by incremental and local deformation, due to its advantages such as considerable savings in energy and material costs, high quality and high efficiency [1–3].

In hot ring rolling, microstructure of the ring has an interactive effect on the thermal and mechanical behaviors, and meanwhile undergoes complex changes such as static and dynamic recrystallization and grain growth [4]. The performance and reliability of the ring product have a close relationship with the final microstructure, which depends heavily on the microstructure evolution history and processing parameters [5]. However, the final microstructure of the large ring is particularly difficult to control because the large ring is generally made of challenging materials such as titanium alloy, superalloy, and aluminum alloy which have poor formability and strong dependence upon both temperature and strain rate [6] on the one hand and, on the other hand, the large size (the external diameter of the large ring product is generally greater than 1 m) of the ring readily causes to form non-uniform microstructure and performance. At present, rapidly developing aviation and space industries have an increasingly stringent demand for the performance and reliability of the large ring product, so it is an important and urgent issue to

gain an insight into the microstructure evolution of the large ring in hot ring rolling, which needs to perform microstructure evolution modeling first.

Modeling of microstructure evolution based on FEM is higher in accuracy than the analytical method and cheaper in cost than the experimental method. Moreover, it can solve some problems which are beyond the capability of the analytical or experimental method, so it has become a hot and challenging topic in the frontier of the advanced plastic forming field [7]. Until now, FE modeling of microstructure evolution during hot forming processes has focused on traditional rolling and forging. Lin et al. [8] incorporated mechanism-based microstructure parameters into a visco-plastic flow model to form a set of unified constitutive equations, which are implemented into the FE solver ABAQUS/Standard through the user defined subroutine CREEP, to simulate microstructure evolution in hot forming processes such as Ti–6Al–4V superplastic forming and hot rolling of carbon steel. Ding et al. [9] developed a constitutive model and a dynamic recrystallization model of AM50 alloy by means of tension and compression tests at elevated temperature, and applied the models to DEFORM-3D for investigating recrystallized grains and recrystallized fraction of AM50 alloy rolled at different temperatures and roller speeds. Hu et al. [10] established a constitutive model and microstructure evolution model of Ti–6Al–4V in the two-phase field, and incorporated them into a coupled thermal–plastic 2D-FE model of hot die forging of aerofoil blade in ABAQUS/Standard, to predict β phase volume fraction and grain size on typical sections of blade before and after forging. Ding et al. [11] coupled a mesoscopic dislocation-based model with a macroscopic FE analysis through the user material subroutine UMAT in ABAQUS/Standard for concurrent study of local plastic flow and microstructure of Ti–6Al–4V in the (α+β) phase field during thermomechanical deformation, with consideration of the effects of local dislocation density variation, deformation heating and phase volume fraction.

These works are helpful for microstructure evolution modeling for hot ring rolling, but very little has been done regarding the latter until now. Xu et al. [12] imbedded a microstructure evolution model of carbon steel into a coupled thermomechanical rigid-plastic 3D-FE code, and obtained α grain size and its distribution at the deformation zone and on seven cross-sections outside the deformation zone. But the study assumed a steady metal flow in the deformation zone, which is not consistent with the essence of the process. In addition, only the microstructure on partial cross-sections can be obtained, so it is difficult to realize an accurate and comprehensive analysis using the code. Sun et al. [13] revealed the influences of processing parameters on recrystallized α grain size and volume fraction of AISI5140 steel in hot ring rolling using the built-in microstructure module of DEFORM-3D. Yeom et al. [14] combined a microstructure model of Ti–6Al–4V with a 3D-FE model of hot rolling of large ring, to predict the α phase grain size and volume fraction. However, all the above microstructure modeling for hot ring rolling are treated as post processor, therefore it fails to realize the coupled simulation between microstructure evolution and thermal and mechanical behaviors.

In the present study, a microstructure evolution subroutine of titanium alloy is developed through the user material subroutine VUMAT in ABAQUS/Explicit using the implicit integration algorithm, thus realizing microstructure evolution modeling coupled with macroscopic thermal and mechanical behaviors. The developed subroutine is imbedded into a coupled thermomechanical 3D-FE model for hot rolling of Ti–6Al–4V large ring. The characteristics of microstructure evolution and the final microstructure of the large ring under different processing parameters are investigated.

2 Numeralization of microstructure evolution of titanium alloy

2.1 Mathematical models

2.1.1 Microstructure evolution model of titanium alloy

Hu et al. [10] established a microstructure evolution model of Ti–6Al–4V in two-phase field. The model believes that the deformation behavior in the temperature range of 800–950 °C is predominately a function of the β phase grain size and volume fraction, with the grain size effects of the α phase being relatively small. The microstructure evolution model of Hu et al. [10] is summarized as follows: the β volume fraction V_f can be expressed as a simple Arrhenius relationship

$$V_f = Ce^{Q_\beta/RT} \tag{1}$$

here Q_β is the activation energy for the β phase stability, which is close to half the activation energy for diffusion, R the universal gas constant and T the absolute temperature. The initial β grain size before deformation, d_0, can be estimated by an exponential function

$$d_0 = Ke^{Q_g/RT} \tag{2}$$

here Q_g is the activation energy for grain growth, which is similar to that of diffusion. The β grain size after deformation, d, can be expressed by

$$d = d_0 + d_0\left(S_1\lambda^3 + S_2\lambda^2 + S_3\lambda + S_4\right) \quad (3)$$

here λ is an internal state variable closely related to the degree of recrystallization, which varies towards the steady-state structure, λ_{ss}, exponentially with the equivalent plastic strain $\bar{\varepsilon}^p$, that is

$$\lambda = \lambda_{ss} + (1 - \lambda_{ss})e^{-\alpha\bar{\varepsilon}^p} \quad (4)$$

λ_{ss} depends on the Zener–Hollomon parameter Z by a power law

$$\lambda_{ss} = \lambda_0 Z^{q_1} \quad (5)$$

Z can be calculated according to

$$Z = \dot{\bar{\varepsilon}}^p e^{Q_{demf}/RT} \quad (6)$$

Here, $\dot{\bar{\varepsilon}}^p$ is the equivalent plastic strain rate, Q_{defm} the activation energy for deformation, and C, Q_β, K, Q_g, $S_1 \sim S_4$, α, λ_0, q_1, Q_{defm} and R in Eqs.(1), (2), (3), (4), (5), and (6) are constants, with their values listed in Table 1.

2.1.2 Constitutive model of titanium alloy

A constitutive model of Ti–6Al–4V in two-phase field can be described by [10]

Table 1 Values of constants in microstructure and constitutive models of Ti–6Al–4V [10]

Constant	Value
Microstructure model	
C	1.476E3
$Q_\beta/R/^\circ$C	−9.0914E3
K/μm	1.9E6
$Q_g/R/^\circ$C	−1.45E4
S_1	6.4312E2
S_2	−1.5501E3
S_3	1.2686E3
S_4	−3.7187E2
α	6.07
λ_0/s	6.424
q_1	−5.17E-2
$Q_{\mathrm{defm}}/R/^\circ$C	5.0668E4
Constitutive model	
k	4.96E-4
m	3E-1
n	1
β_1	6.673E1

$$\sigma^y = kZ^m\lambda^n\left(1 - e^{-\beta_1\bar{\varepsilon}^p}\right) \quad (7)$$

here σ^y is the yield stress, Z the Zener–Hollomon parameter, λ the internal state variable which reflecting the influence of microstructure on deformation, and k, m, n, and β_1 are constants and their values for Ti–6Al–4V have been determined by experiments, as shown in Table 1.

2.2 Development of microstructure evolution subroutine

The constitutive model of Ti–6Al–4V described by Eq. (7) is integrated implicitly based on the elastic–predictor plastic–corrector scheme [15]. According to the constitutive integration algorithm, the microstructure evolution model and the rate-/temperature-/microstructure-dependent elastic–plastic constitutive model of titanium alloy are implemented in ABAQUS/Explicit through the user material subroutine VUMAT, and thus the simulation is realized with respect to microstructure evolution coupled with mechanical and thermal behaviors. The flow chart of the microstructure evolution subroutine is shown in Fig. 1.

2.3 Validation of microstructure evolution subroutine

The microstructure evolution subroutine is unconditionally stable since the constitutive model is integrated implicitly. In the following, the reliability of the subroutine is validated first by single-element models and then by isothermal upsetting experiments of Ti–6Al–4V cylinder.

2.3.1 Single-element models

The coupled thermomechanical 3D-FE model of a single-element under compression or shear deformation is used to validate the subroutine first, because the single-element model has simple geometry, specific loading and high computational efficiency. The element type is C3D8RT with an only integration point locating at the geometrical center of the element. The side length of the element is 1 mm, the loading velocity is 10 mm/s, the loading time is 0.01 s and the initial temperature of the element is 880 °C. The simulation results of compression and shear deformation of the element by using the subroutine are shown in Figs. 2 and 3, respectively. Comparisons of simulation results of compression and shear deformation between by using the subroutine and by using the built-in routine of ABAQUS/Explicit are shown in Tables 2 and 3, respectively. It can be seen from Figs. 2 and 3, and Tables 2 and 3 that the results obtained from the subroutine agree well with the ones obtained from the built-in routine, which proves that the developed subroutine can accurately predict thermal and mechanical parameters.

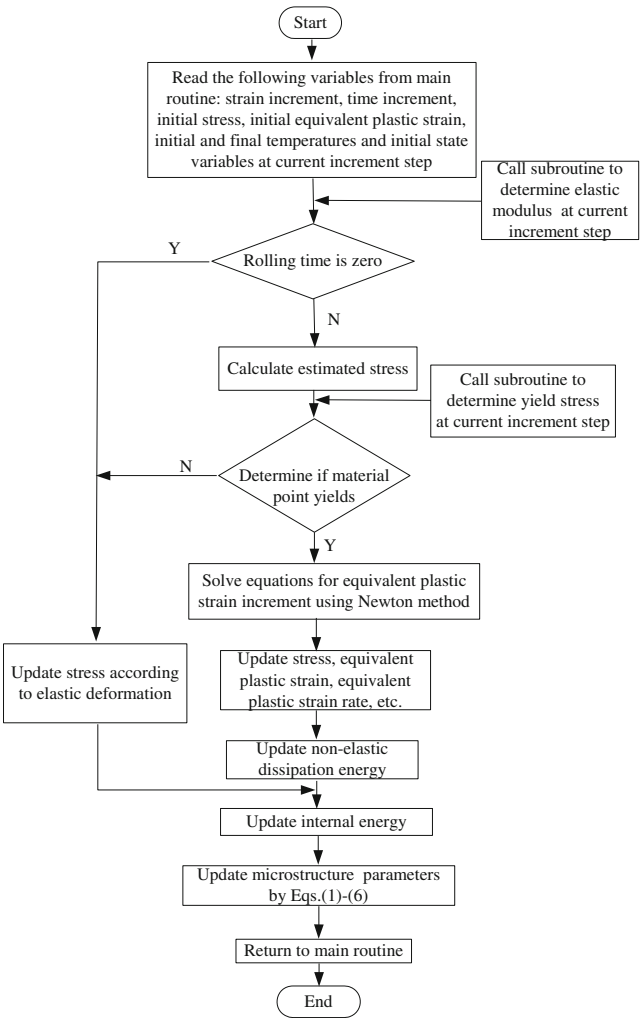

Fig. 1 Flow chart of microstructure evolution subroutine

2.3.2 Isothermal upsetting experiments of Ti–6Al–4V cylinder

Isothermal upsetting experiments of Ti–6Al–4V cylinder described in Ref. [16] is used to further validate the subroutine. The initial size of the cylinder is Φ8×12 mm, the velocity of the upper die is 0.1 mm/s and the friction coefficient between the die and cylinder is 0.3. When the reduction ratio is 39.14 % and deformation temperature is 920 °C, the distributions of the equivalent plastic strain and β phase volume fraction V_f are shown in Fig. 4. In Fig. 4a, there are typical three deformation zones occurring in the cylinder upsetting experiment [17], namely, difficult deformation zone, large deformation zone and small deformation zone. It can be seen from Fig. 4b that the large and small deformation zones have larger V_f than the difficult deformation zone, with the minimum value appearing at the center of the top and bottom of the cylinder. The predicted V_f at the center of the top (marked by point A) is 82.40 % and the

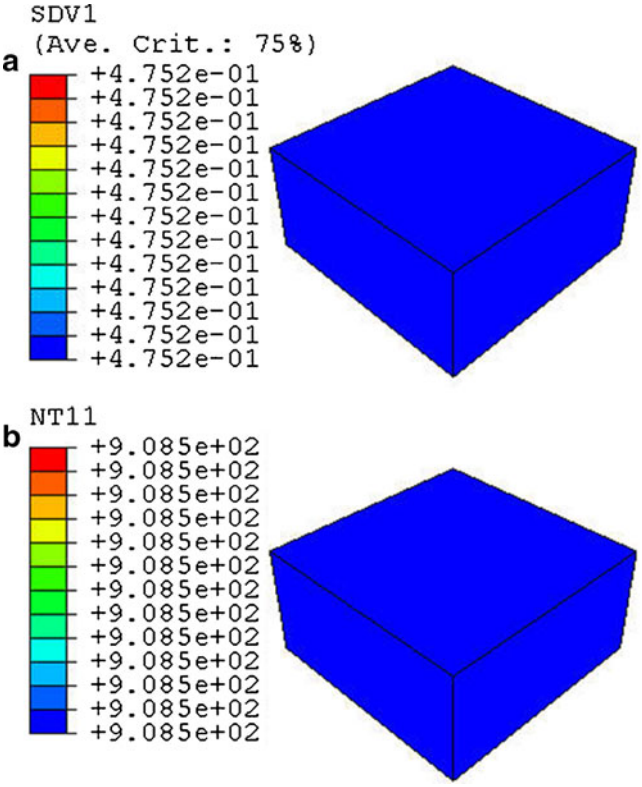

Fig. 2 Simulation results of compression deformation of the single element by using subroutine. **a** equivalent plastic strain; **b** temperature (°C)

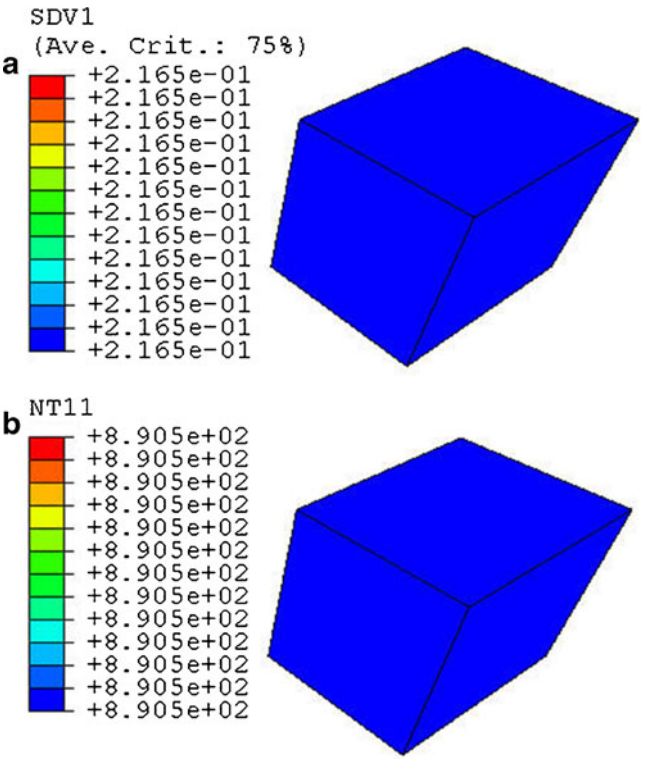

Fig. 3 Simulation results of shear deformation of the single element by using subroutine. **a** Equivalent plastic strain; **b** temperature (°C)

Table 2 Comparison of simulation results of compression deformation between by using the subroutine and by using the built-in routine

	Subroutine	Built-in routine	Relative error (%)
Equivalent plastic strain	0.4752	0.4751	0.02
Temperature/°C	908.5	911.9	−0.37

measured value is 84.86 % [16], with the relative error being −2.9 %. When the reduction ratio is 39.14 %, a comparison between predicted and measured V_f at point A at different temperatures is shown in Table 4. When the deformation temperature is 890 °C, a comparison between predicted and measured V_f at point A at different reduction ratios is shown in Table 5. It can be found from Tables 4 and 5 that the absolute value of the maximum relative error between predicted and measured values is not beyond 10%, which demonstrates that the developed microstructure evolution subroutine is reliable. In addition, it is observed that the predicted values of V_f are always less than the measured ones. The reason for this may be that poor lubrication in the experiment causes the friction coefficient between the die and cylinder to increase and consequently, the top and bottom of the cylinder have a higher temperature due to heat generated from friction, leading to the increase in V_f.

3 Results and discussion

3.1 Microstructure evolution modeling of titanium alloy large ring in hot ring rolling

Under the computational conditions shown in Table 6, a coupled thermomechanical 3D-FE model for hot rolling of titanium alloy large ring is established using the modeling method developed by authors [18], as shown in Fig. 5. The model has been validated by a comparison between the numerical result and experimental one in terms of surface temperature and geometry histories [19]. By incorporating the developed microstructure evolution subroutine into the model, a coupled simulation can be realized between microstructure evolution and macroscopic thermal and mechanical behaviors. In the following, the evolution characteristics

Table 3 Comparison of simulation results of shear deformation between by using the subroutine and by using the built-in routine

	Subroutine	Built-in routine	Relative error (%)
Equivalent plastic strain	0.2165	0.2160	0.23
Temperature/°C	890.5	892.1	−0.18

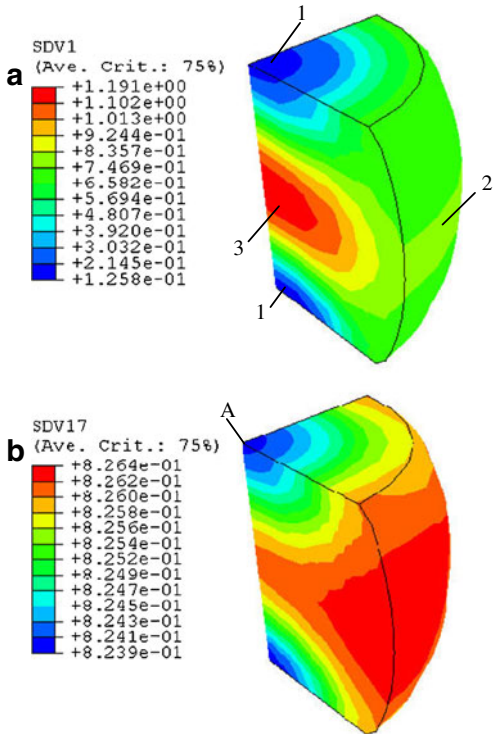

Fig. 4 Distributions of field variables in Ti–6Al–4V cylinder (only a quarter is displayed) after isothermal upsetting. **a** Equivalent plastic strain; **b** β volume fraction V_f

of β grain size and volume fraction of the Ti–6Al–4V large ring are revealed, and the final microstructures of the large ring under different processing parameters are explored.

3.2 Characteristics of microstructure evolution of titanium alloy large ring

Figure 6 illustrates the evolution of the β grain size d. It can be seen that the d in the deformation zone is always smaller than that outside the deformation zone. This is because the deformation zone has a larger strain rate, which makes the dislocation density increase and thus the dynamic recrystallization degree increase on the one hand and, on the other hand, causes the recrystallized grain to have not enough time to grow. The discrepancy between microstructures inside and outside the deformation zone will generally

Table 4 Comparison between predicted and measured [16] values of β volume fraction V_f at point A at different temperatures

Temperature /°C	Predicted value /%	Measured value/%	Relative error/%
860	61.28	62.15	−1.40
890	68.21	70.46	−3.19
920	82.40	84.86	−2.90

Table 5 Comparison between predicted and measured [16] values of β volume fraction V_f at point A at different reduction ratios

Reduction ratio /%	Predicted value/%	Measured value/%	Relative error/%
25.77	63.72	70.05	−9.04
39.14	68.21	70.46	−3.19

disappear in practice because the rolling stage is followed by a reforming stage in which the strain rate decreases gradually to zero. The reforming stage is not considered in the study for computational time saving. It is also observed from Fig. 6 that the fine grain zone first appears in the deformation zone (Fig. 6a), and then extends gradually along the circumferential direction of the ring (Fig. 6b). After the first rotation of the ring, d has an axisymmetric distribution (Fig. 6c~d). Moreover, at the early stage, the d in the surface layer (SL, which consists of the inside and outside layers along the radial direction, as shown in Fig. 6b) decreases sharply, resulting in the fine grain zone locating at the SL and the coarse grain zone existing in the middle layer (ML) (Fig. 6a~b). This is because the SL has larger strain rate and strain relative to the ML. Larger strain causes the dislocation density and thus the distortion energy to increase, leading to the increased recrystallization driving force and the onset of recrystallization. Afterwards, the d in the SL increases whereas that in the ML decreases (Fig. 6c), which makes the fine grain zone, at the later stage, transfer to the ML while the coarse grain zone transfer to the outside layer (Fig. 6d). The reason for this is that the SL has a larger

Table 6 Computational conditions for hot rolling of Ti–6Al–4V large ring

Forming parameter	Value
Reduction ratio/ %	53.3
Rotational velocity of driver roll/ rad/s	8.21
Feed rate of idle roll/ mm/s	5
Initial temperature of ring/ °C	880
Friction coefficient	0.5
Temperature of rolls/ °C	250
Temperature of environment/ °C	30
Contact heat conductivity/ W/(m^2°C)	4,000 [21]
Convection coefficient/ W/(m^2°C)	20 [22]
Emissivity	0.6 [22]
Radius of driver roll/ mm	225
Radius of idle roll/ mm	160
Radius of guide rolls/ mm	160
Initial outer radius of ring/ mm	397.5
Initial inner radius of ring/ mm	210
Initial axial height of ring/ mm	80

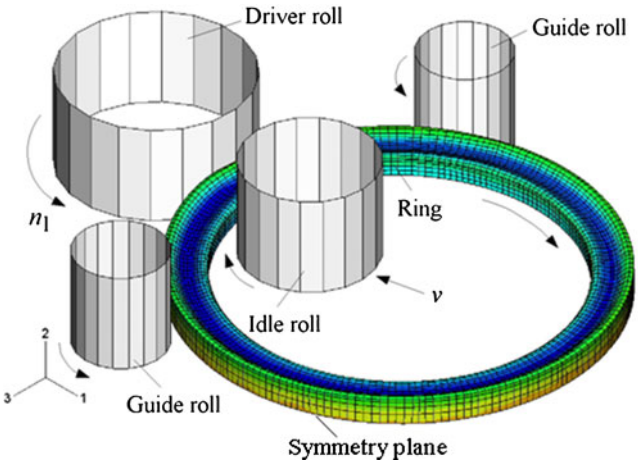

Fig. 5 Coupled thermomechanical 3D-FE model for hot rolling of titanium alloy large ring

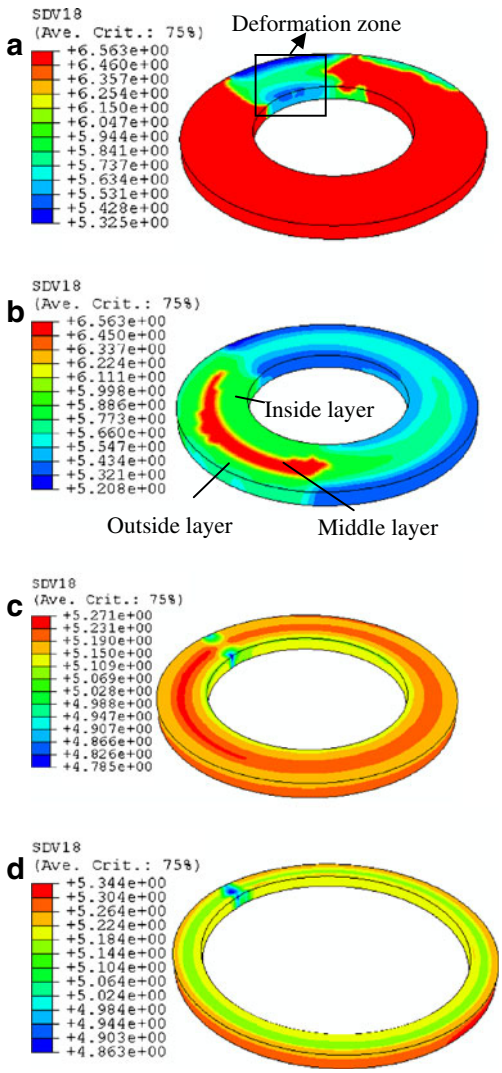

Fig. 6 Evolution of β grain size d (μm). **a** t=0.8 s; **b** t=1.6 s; **c** t=9.6 s; **d** t=20 s

temperature rise, which promotes grain boundaries activity and increases the migration rate of grain boundaries, making the grain grow faster. The ML has a smaller temperature rise and furthermore, both strain and strain rate increase, causing the d in the ML to decrease.

The evolution of β volume fraction V_f is shown in Fig. 7. It is observed from Fig. 7 that like d, V_f changes in the deformation zone first (Fig. 7a). Then, it extends gradually along the circumferential direction of the ring (Fig. 7b). After the first rotation of the ring, V_f has an axisymmetric distribution (Fig. 7c~d). It can also be seen that at the early stage, the large V_f zone (the rich β zone) locates at the outside layer of the ring, and the small V_f zone (the poor β zone) exists at the surface of the inside layer (Fig. 7a~b). Afterwards, the SL is larger in the increase of V_f than the ML (Fig. 7c), which makes at the later stage, the rich β zone still locates at the outside layer, and the poor β zone extends from the surface of the inside layer to the end-plane of the ML(Fig. 7d). The evolution of V_f relies heavily on the temperature, i.e., the higher the temperature, the more the α phase transforming into β phase, leading to increased V_f. The predicted location of the poor β zone in deformed ring is in good agreement with the experimental result obtained by Yeom et al. [14], but there exists difference relative to the location of the rich β zone. Yeom et al. [14] observed in experiment that the rich β zone locates at the ML instead of the SL predicted by the study. The reason may be that under the forming conditions in the study, the plastic deformation does not completely penetrate the radial thickness of the ring, so the large deformation zone occurs in the SL, causing the SL to have higher temperature [20]. In contrast, the plastic deformation completely penetrates the radial thickness in the experiment of Yeom et al. [14], and thus the large deformation zone occurs in the ML, making the ML have higher temperature.

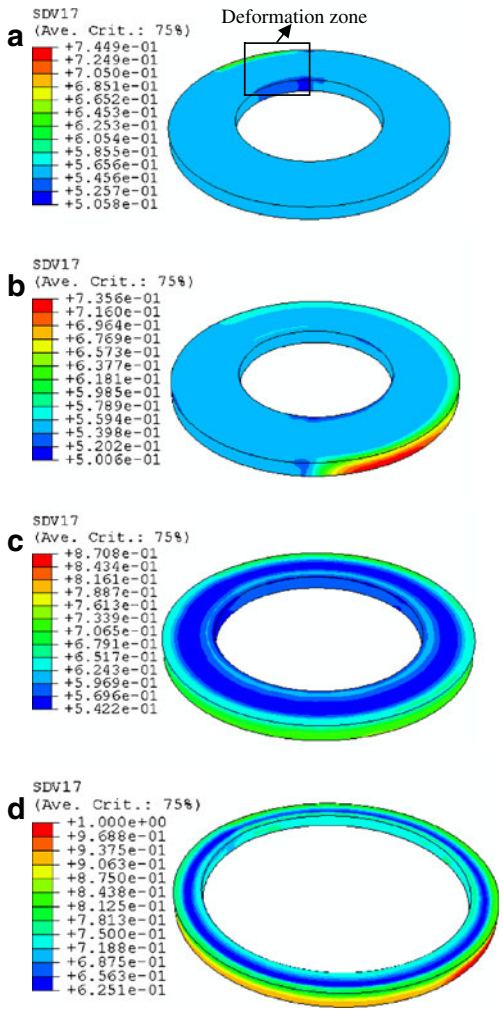

Fig. 7 Evolution of β volume fraction V_f. **a** 0.8 s; **b** 1.6 s; **c** 9.6 s; **d** 20 s

3.3 Final microstructures of titanium alloy large ring under different processing parameters

3.3.1 Characterization indexes of microstructure

The paper adopts the following characterization indexes to evaluate the quality of the final microstructure of the large ring.

1. Average β grain size of the ring, d_a

$$d_a = \sum_{i=1}^{N} (d_i \cdot V_i) \Big/ \sum_{i=1}^{N} V_i$$

here N is the number of elements of the ring, and d_i and V_i are the β grain size and volume fraction at element i, respectively. The smaller the d_a, the finer the β grain size of the ring overall.

2. The uniformity of β grain size distribution, SDD

$$\mathrm{SDD} = \sqrt{\sum_{i=1}^{N} \left((d_i - d_a)^2 \cdot V_i \right) \Big/ \sum_{i=1}^{N} V_i}$$

The less the SDD, the more uniform the β grain size distribution.

3. Average β volume fraction of the ring, V_{fa}

$$V_{fa} = \sum_{i=1}^{N} (V_{fi} \cdot V_i) \Big/ \sum_{i=1}^{N} V_i$$

here V_{fi} is the volume fraction at element i. The less the V_{fa}, the less the β phase of the ring overall.

4. The uniformity of β phase distribution, SDV

$$\mathrm{SDV} = \sqrt{\sum_{i=1}^{N}\left((V_{\mathrm{f}i} - V_{\mathrm{f}a})^2 \cdot V_i\right) \Big/ \sum_{i=1}^{N} V_i}$$

The less the SDD, the more uniform the β phase distribution.

3.3.2 Rotational velocity of driver roll n_1

Figure 8 shows the variation of the β grain size d with n_1. In Fig. 8a, both the average β grain size d_a and the uniformity of β grain size distribution SDD increase with n_1 increasing, which indicates that the β grain size of the ring becomes larger overall, and meanwhile its distribution tends to become more non-uniform. This is due to that as n_1 increases, the d in the SL increases while that in the ML nearly holds unchanged, as shown in Fig. 8b. This change of d distribution along the radial direction under different n_1 is the combined effects of the changes of temperature, strain and strain rate distributions according to Eqs. (2) - (6).

The variation of the β volume fraction V_f with n_1 is shown in Fig. 9. It can be seen from Fig. 9a that both the average volume fraction V_{fa} and the uniformity of β phase distribution SDV increase with n_1 increasing, which implies that the β phase increases, and its distribution tends to be non-uniform. The reason for this is that as n_1 increases, the SL rises while the ML slightly drops in temperature [20], causing the V_f in the SL to increase while that in the ML to decrease a little, as shown in Fig. 9b.

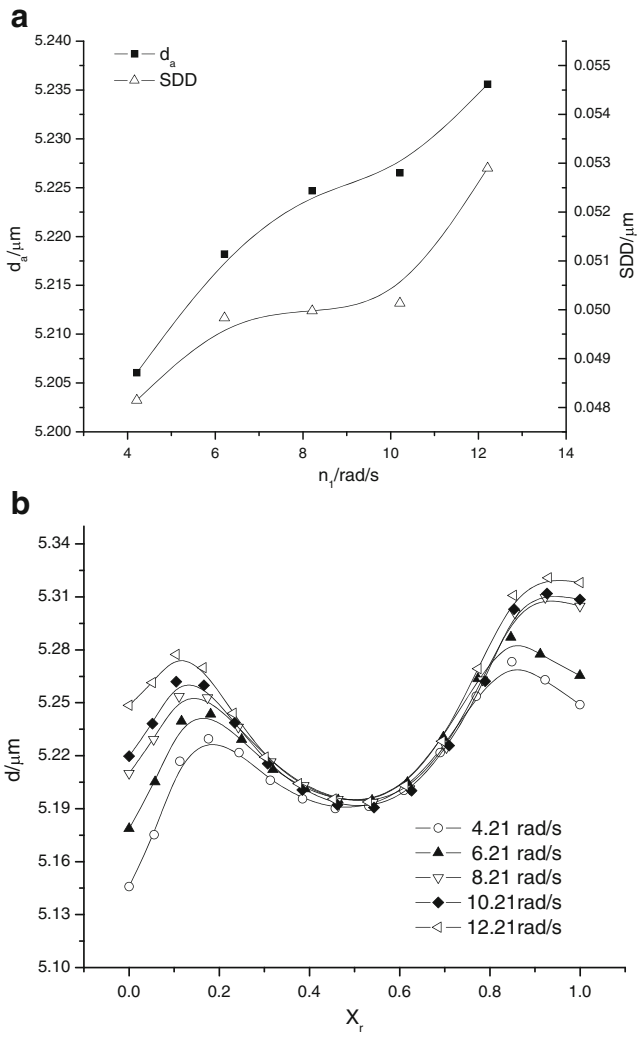

Fig. 8 Variation of β grain size d with rotational velocity of driver roll n_1. **a** average grain size d_a and uniformity of β grain size distribution SDD; **b** d distribution along radial direction of ring

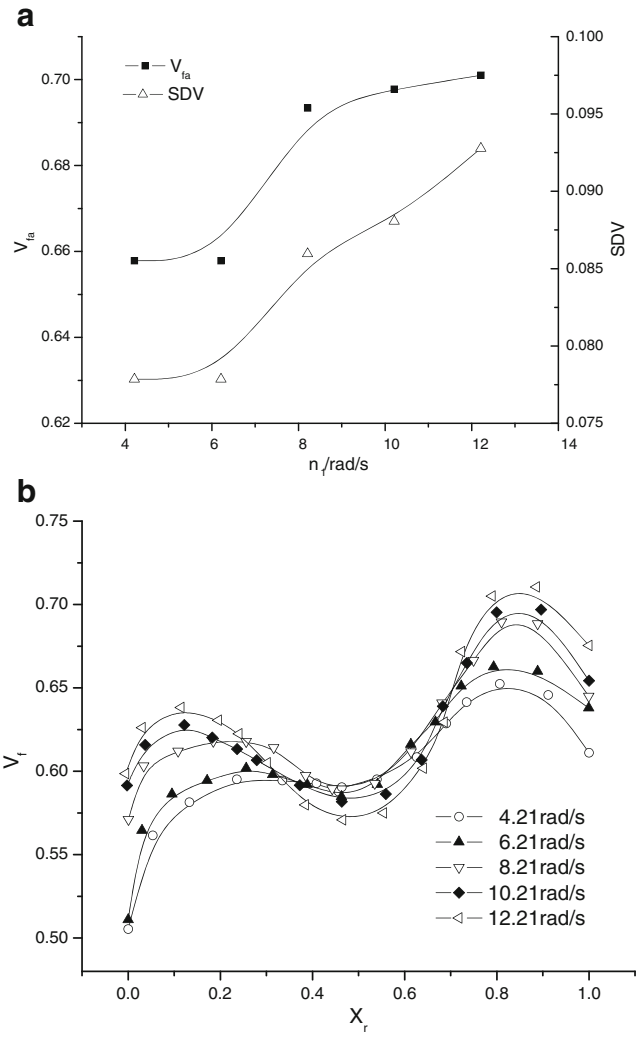

Fig. 9 Variation of β volume faction V_f with rotational velocity of driver roll n_1. **a** average β volume fraction V_{fa} and uniformity of β phase distribution SDV; **b** V_f distribution along radial direction of ring

3.3.3 Feed rate of idle roll v

The variation of the d with v is shown in Fig. 10. From Fig. 10a, it is observed that as v increases, the d_a slightly increases and the SDD has a little change. This demonstrates that the β grain size of the ring increases a little and its distribution almost remains unchanged, which is caused by the fact that with v increasing, the d in the SL slightly increases while that in the ML holds nearly unchanged, as shown in Fig. 10b.

Figure 11 shows the variation of the V_f with v. In Fig. 11a, the V_{fa} increases and the SDV decreases with v increasing. This implies that the β phase increases, and its distribution tends to be more uniform, which arises from that as v increases, the SL has a smaller temperature rise than the ML [20], making the SL have a smaller increase of V_f than the ML, as shown in Fig. 11b.

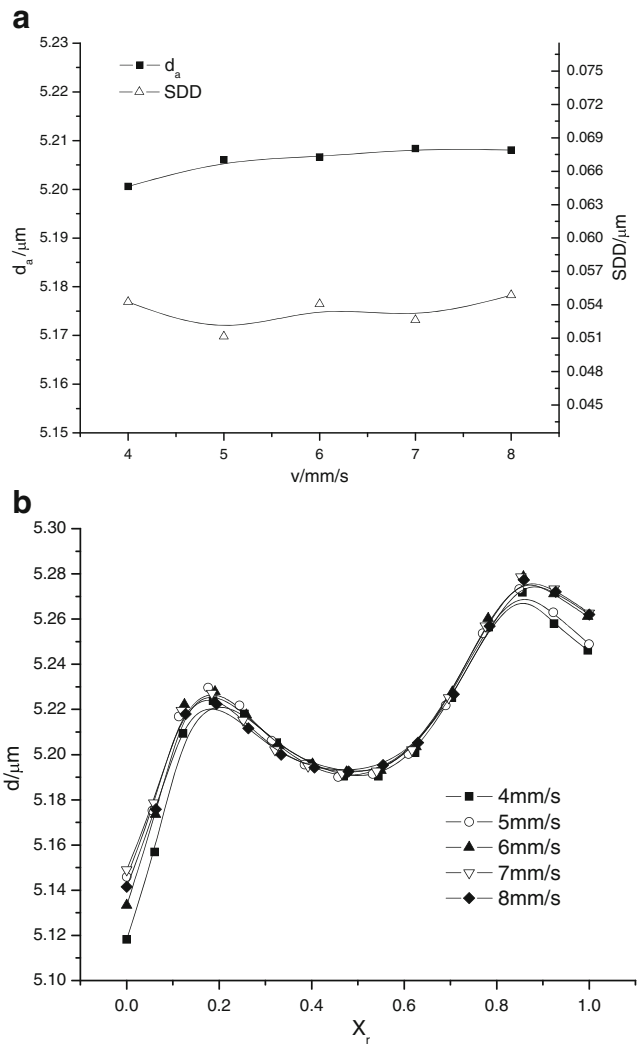

Fig. 10 Variation of β grain size d with feed rate of idle roll v. **a** average grain size d_a and uniformity of β grain size distribution SDD; **b** d distribution along radial direction of ring

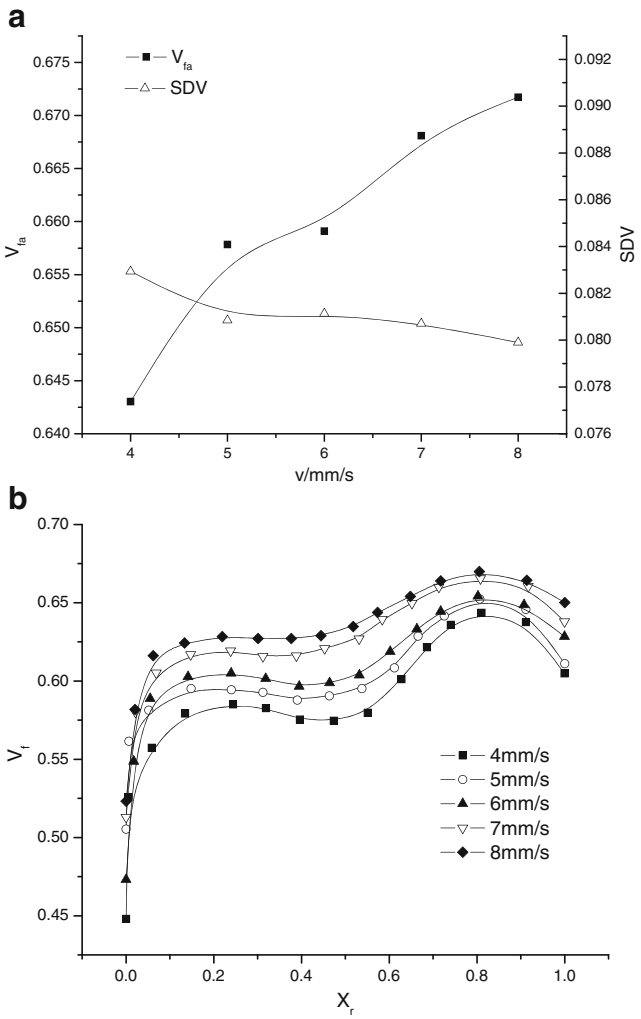

Fig. 11 Variation of β volume fraction V_f with feed rate of idle roll v. **a** average β volume fraction V_{fa} and uniformity of β phase distribution SDV; **b** V_f distribution along radial direction of ring

3.3.4 Initial temperature of ring T_0

The variation of the d with T_0 is shown in Fig. 12. It is found from Fig. 12a that the d_a increases and the SDD decreases with T_0 rising, which indicates that the β grain size of the ring increases overall and its distribution tends to be more uniform. This may result from the SL having a smaller increase of d than the ML as T_0 rises, which is not obvious in Fig. 12b. This is because the change of d with T_0 is considerably larger than that with the radial location.

The variation of the V_f with T_0 is shown in Fig. 13. It can be seen from Fig. 13a that the V_{fa} increases and the SDV decreases with T_0 rising, which demonstrates that the β phase increases and its distribution tends to be more uniform. This is caused as T_0 rises, the SL is smaller in temperature rise than the ML [20], leading to the V_f in the SL having a smaller increase than that in the ML, as shown in Fig. 13(b).

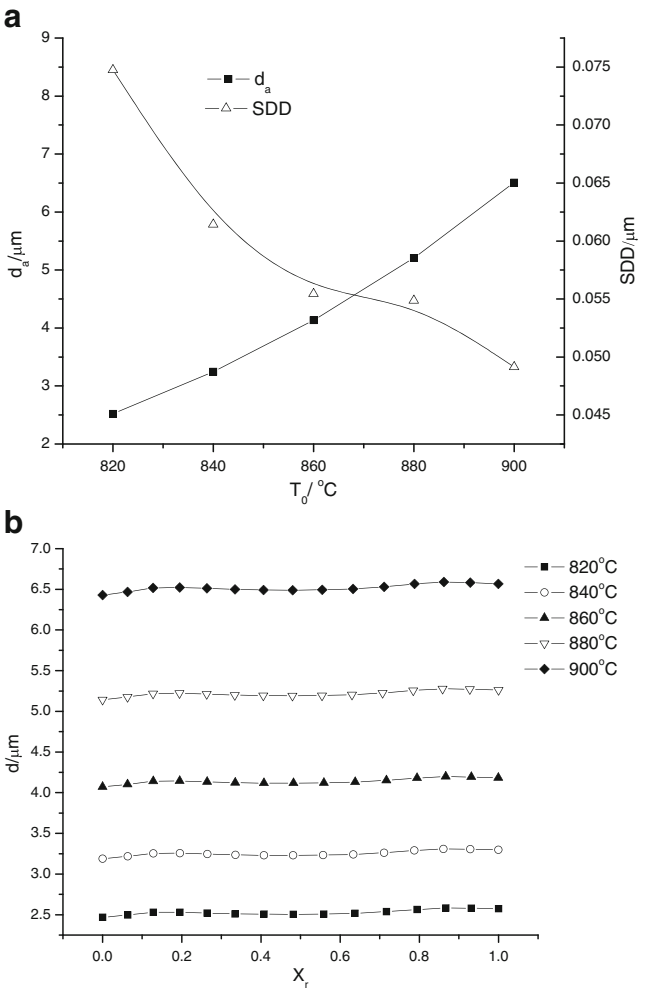

Fig. 12 Variation of β grain size d with initial temperature of ring T_0. **a** average grain size d_a and uniformity of β grain size distribution SDD; **b** d distribution along radial direction of ring

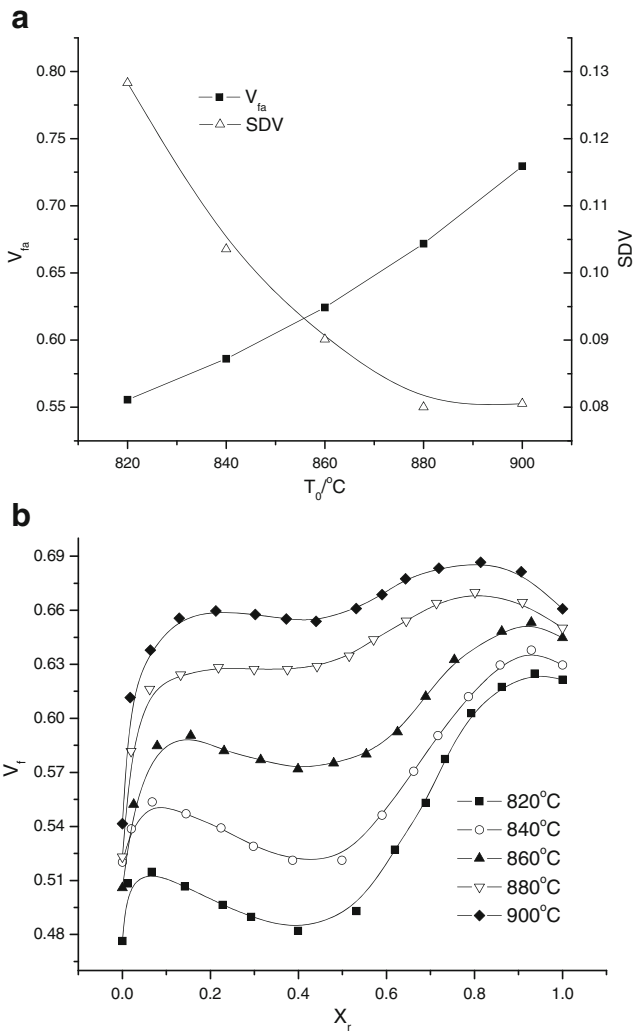

Fig. 13 Variation of β volume fraction V_f with initial temperature of ring T_0. **a** average β volume fraction V_{fa} and uniformity of β phase distribution SDV; **b** V_f distribution along radial direction of ring

4 Conclusions

The microstructure evolution model and the rate-/temperature-/microstructure-dependent elastic–plastic constitutive model of titanium alloy are implemented in ABAQUS/Explicit through the user material subroutine VUMAT by using the implicit integration algorithm, thus realizing microstructure evolution simulation coupled with mechanical and thermal behaviors. The developed microstructure evolution subroutine is imbedded into a coupled thermomechanical 3D-FE model for hot rolling of Ti–6Al–4V large ring. The evolution characteristics of β phase grain size and volume fraction of titanium alloy are revealed and the final microstructures of the large ring under different processing parameters are explored. The results obtained are as follows:

1. Microstructure evolution follows the trend with the process progressing: the fine grain zone transfers from the SL to the ML of the ring; the poor β zone extends from the outside of the SL to the end-plane of the ML, and the rich β zone always locates at the SL.
2. Decreasing the rotational velocity of the driver roll n_1, or increasing the feed rate of the idle roll v or the initial temperature of the ring T_0 contributes to more uniform distributions of β phase and its grain size, but results in the increase in the β phase volume fraction and grain size.

The study can provide a theoretical basis for microstructure control and performance improvement of titanium alloy large ring in hot ring rolling, and may serve as a guide to microstructure evolution modeling for relevant metal-forming processes.

Acknowledgments The authors would like to thank the National Natural Science Foundation for Key Program of China (50935007), National Natural Science Foundation for General Program of China (50805120, 50905056), National Major Projects for Science and

Technology Development (2009ZX04014-074-03) and Material Forming and Mould Technology Open State Key Laboratory of Funded Projects (2012-P12) for the support given to the research.

References

1. Allwood JM, Kopp R, Michels D, Music O, Öztop M, Stanistree TF, Tekkaya AE, Tiedemman I (2005) The technical and commercial potential of an incremental ring rolling process. CIRP Ann Manuf Technol 54:233–236
2. Yang H, Fan XG, Sun ZC, Guo LG, Zhan M (2011) Recent development in plastic forming technology of titanium alloys. Sci China SER E 54:490–501
3. Hua L, Huang XG, Zhu CD (2001) Theory and technology of ring rolling. China Machine Press, Beijing (in Chinese)
4. Ma Q, Lin ZQ, Yu ZQ (2009) Prediction of deformation behavior and microstructure evolution in heavy forging by FEM. Int J Adv Manuf Technol 40:253–260
5. Zhou J, Wang FL, Wang MH, Xu WJ (2011) Study on forming defects in rolling process of large aluminum alloy ring via adaptive controlled simulation. Int J Adv Manuf Technol 55:95–106
6. Dunne FPE (1998) Inhomogeneity of microstructure in superplasticity and its effect on ductility. Int J Plasticity 14:413–433
7. Soppa E, Schmauder S, Fischer G, Thesing J, Ritter R (1999) Influence of the microstructure on the deformation behaviour of meta-matrix composites. Comput Mater Sci 16:323–332
8. Lin J, Dean TA (2005) Modelling of microstructure evolution in hot forming using unified constitutive equations. J Mater Process Tech 167:354–362
9. Ding HL, Hirai K, Homma T, Kamado S (2010) Numerical simulation for microstructure evolution in AM50 Mg alloy during hot rolling. Comput Mater Sci 47:919–925
10. Hu ZM, Brooks JW, Dean TA (1999) Experimental and theoretical analysis of deformation and microstructural evolution in the hot-die forging of titanium alloy aerofoil sections. J Mater Process Tech 88:251–265
11. Ding R, Guo ZX, Qian M (2007) Coupled mesoscopic constitutive modelling and finite element simulation for plastic flow and microstructure of two-phase alloy. Comput Mater Sci 40:201–212
12. Xu SG, Cao QX (1994) Numerical simulation of the microstructure in the ring rolling of hot steel. J Mater Process Tech 43:221–235
13. Sun ZC, Yang H, Ou XZ (2010) Effects of process parameters on microstructural evolution during hot ring rolling of AISI 5140 steel. Comput Mater Sci 49:134–142
14. Yeom JT, Kim JH, Hong JK, Park NK, Lee CS (2010) FE analysis of microstructure evolution during ring rolling process of a large-scale Ti–6Al–4V ring. Mater Sci Forum v 638–642:223–228
15. Fotiu PA, Nasser SN (1996) A universal integration algorithm for rate-dependent elastoplasticity. Comput Struct 59:1173–1184
16. Nie L, Li FG, Fang Y (2002) Process simulation and microstructure prediction of Ti–6Al–4V alloy in isothermal forging. Aerospace Materials & Technology: 45–49 (in Chinese)
17. Wang DN (1982) Metal plastic forming theory. China Machine Press, Beijing (in Chinese)
18. Wang M, Yang H, Sun ZC, Guo LG (2006) Dynamic explicit FE modeling of hot ring rolling process. T Nonferr Metal Soc 16:1274–1280
19. Yang H, Wang M, Guo LG, Sun ZC (2008) 3D coupled thermo-mechanical FE modeling of blank size effects on the uniformity of strain and temperature distributions during hot rolling of titanium alloy large ring. Comput Mater Sci 44:611–621
20. Wang M, Yang H, Sun ZC, Guo LG (2009) Analysis of coupled mechanical and thermal behaviors in hot rolling of large rings of titanium alloy using 3D dynamic explicit FEM. J Mater Process Tech 209:3384–3395
21. Hu ZM, Brooks JW, Dean TA (1998) The interfacial heat transfer coefficient in hot die forging of titanium alloy. Proc ImechE 212:485–496
22. Lee RS, Lin HC (1998) Process design based on the deformation mechanism for the non-isothermal forging of Ti–6Al–4V alloy. J Mater Process Tech 79:224–235